X-ray Microscopy of Photovoltaic Polyfluorene Blends: Relating Nanomorphology to Device Performance

Christopher R. McNeill,*,† Benjamin Watts,‡ Lars Thomsen,§ Harald Ade,‡ Neil C. Greenham,† and Paul C. Dastoor§

Cavendish Laboratory, Department of Physics, University of Cambridge, J J Thomson Avenue, Cambridge CB3 0HE, United Kingdom; Department of Physics, North Carolina State University, Raleigh, North Carolina 27695; and School of Mathematical and Physical Sciences, University of Newcastle, University Drive, Callaghan NSW 2308, Australia

Received January 17, 2007; Revised Manuscript Received February 23, 2007

ABSTRACT: The composition of blend films of poly(9,9′-dioctylfluorene-*co*-bis-*N*,*N*′-(4-butylphenyl)-bis-*N*,*N*′-phenyl-1,4-phenylenediamine) (PFB) and poly(9,9′-dioctylfluorene-*co*-benzothiadiazole) (F8BT) used in prototype polymer solar cells has been quantitatively mapped using scanning transmission X-ray microscopy (STXM). The resolution of the STXM technique is 50 nm or better, allowing the first nanoscale lateral chemical mapping of this blend system. For 1:1 blend films spin-coated from xylene we find that the F8BT-rich domain is over 90% pure (by weight) and the PFB-rich domain contains 70% PFB. For 5:1 and 1:5 blend films processed from xylene, the minority phases are found to be intermixed, containing as much as 50% by weight of the majority polymer. Films prepared from chloroform with a 1:1 weight ratio have also been imaged but show no features on the length scale of 50 nm or greater. Additionally, the performance of photovoltaic devices fabricated using films prepared in an identical fashion to those prepared for STXM analysis has been evaluated and compared to the performance of chloroform blends with varied weight ratio. By studying the influence of blend composition on device performance in chloroform blends with a uniform morphology, we relate the performance of xylene-processed films to the local blend composition measured by STXM and the degree of nanoscale phase separation.

Introduction

Photovoltaic devices based on blends of donor and acceptor conjugated polymers are an attractive route to low-cost solution-processed solar cells.[1,2] Of particular interest to the development of this technology is the influence film morphology upon device performance.[3] Because of the low exciton diffusion length in conjugated polymers (typically less than 10 nm[4]), it is hypothesized that efficient devices require an intimately mixed morphology with phase separation on the length scale of 10 nm but with bicontinuous networks for efficient charge collection.[5] Mixtures of the donor polymer poly(9,9′-dioctylfluorene-*co*-bis-*N*,*N*′-(4-butylphenyl)-bis-*N*,*N*′-phenyl-1,4-phenylenediamine) (PFB) with the acceptor polymer poly(9,9′-dioctylfluorene-*co*-benzothiadiazole) (F8BT) have provided a model system for the study of morphology effects[6−10] and charge generation and transport dynamics in polymer blends.[7,11−14] Blends of PFB and F8BT spin-coated from a low boiling point solvent, such as chloroform, exhibit a smooth surface topography with a fine scale of intermixing on the length scale of tens of nanometers.[6] Films spin-coated from a high boiling point solvent, such as xylene, however, show a more complicated morphology characterized by columnar, micron-sized domains.[15] Although devices based on chloroform blends outperform those from xylene blends, the difference in performance is not as great as would be expected from the very large difference in the characteristic length scale of their respective film morphologies.[6] Snaith et al. linked external quantum efficiency with the interfacial area between the micron-sized domains and hence concluded that the most efficient photocurrent generation mechanism in these blends is the dissociation of excitons at the PFB-rich/F8BT-rich interface followed by charge transport along the columnar structures.[7,10] Recent photocurrent mapping studies, however, revealed that photocurrent collection is most efficient within the micron-sized domains with no evidence of an enhancement at the domain interface.[16] More recently, time-resolved electrostatic force microscopy (EFM) measurements have further supported the photocurrent mapping studies by clearly demonstrating that the domain centers are responsible for the majority of the generated photocurrent.[17]

Understanding the origin of the intradomain charge generation mechanism necessarily requires a technique that is capable of mapping the bulk composition of these blend structures with both high chemical sensitivity and spatial resolution. Although an array of advanced techniques has been used to probe the chemistry and structure of PFB/F8BT blends, none have combined a high chemical sensitivity with a lateral spatial resolution of better than 1 μm.[18,19] Here, we report a systematic scanning transmission X-ray microscopy (STXM) study of the PFB/F8BT system. By measuring near-edge X-ray fine structure (NEXAFS) spectra with an X-ray beam of spot size of 50 nm or better, STXM is uniquely capable of quantitatively mapping the nanoscale chemical composition of polymer blend films. By comparing the STXM compositional maps with the photovoltaic performance of the corresponding organic photovoltaic (OPV) devices, we are able to explain the relative macroscale performance of xylene-processed polyfluorene blends in terms of local nanoscale composition.

Experimental Details

Materials. Poly(9,9′-dioctylfluorene-*co*-bis-*N*,*N*′-(4,butylphenyl)-bis-*N*,*N*′-phenyl-1,4-phenylenediamine) (PFB) and poly(9,9′-dioctylfluorene-*co*-benzothiadiazole) (F8BT) were supplied by

* Corresponding author: Tel +44 (0)1223 337285; Fax +44 (0)1223 764515; e-mail crm51@cam.ac.uk.
† University of Cambridge.
‡ North Carolina State University.
§ University of Newcastle.

10.1021/ma070132d CCC: $37.00
Published on Web 03/30/2007

Cambridge Display Technology Ltd. The molecular weights (M_W) and polydispersities were 135 000 and 2.3 for PFB and 151 000 and 2.4 for F8BT, respectively.

Sample Preparation. Blend solutions were prepared by dissolving each polymer in separate solutions and then mixing these solutions to give the desired weight ratio. Films for STXM analysis were spin-coated onto oxygen plasma-treated glass slides while films for device fabrication were spin-coated from the same solution under identical conditions but on to PEDOT:PSS-coated indium−tin oxide (ITO) glass slides. As both oxygen plasma-treated glass and PEDOT:PSS surfaces are hydrophilic, we expect similar surface segregation effects for films prepared on either substrate. AFM images (Digital Instruments Nanoscope IIIa acquired in noncontact mode) were taken of films on glass and PEDOT:PSS-coated ITO substrates and identical morphologies observed. Since the morphology of laterally phase-separated polymer films is strongly influenced by surface effects,[20] the identical morphologies observed for glass and PEDOT:PSS substrates provides confidence that the same surface segregation effects are seen in both cases. After AFM and thickness measurements (Dektak 6M) were performed, the films were floated off onto deionized water and picked up with copper TEM grids. These grid-supported films were transferred to a nitrogen glovebox to dry. Films spin-coated from *p*-xylene were prepared with weight ratios of 5:1, 1:1, and 1:5 PFB:F8BT while films spin-coated from chloroform were prepared with a weight ratio of 1:1 PFB:F8BT. 1:1 blend films from xylene were spin-coated with thicknesses of 88 nm with a roughness of ±19 nm (as measured by profilometry) by spin-coating at 1500 rpm from solutions with total concentration of 15 g/L. 5:1 and 1:5 blend films from xylene were prepared by spin-coating solutions of concentration 20 g/L at 3000 rpm and 15 g/L at 2000 rpm to give films of thickness 86 ± 3 and 86 ± 2 nm, respectively. Films from chloroform with weight ratio 1:1 were spin-coated from a solution of concentration 8 g/L at 3000 rpm to give a thickness of 80 ± 20 nm (peak-to-peak roughness; while locally smooth the surface of the chloroform films undulates with a period of ∼50 μm.)

STXM Measurements. X-ray microscopy measurements were performed at beamline 5.3.2 of the Advanced Light Source at the Lawrence Berkeley National Laboratory, California.[21] Details of the experiment can be found at length elsewhere.[21] Briefly, the TEM grid-supported films were mounted in the sample chamber which was evacuated to 0.3 mbar and subsequently refilled with $^1/_3$ atm of helium. The transmitted X-ray intensity through the film was recorded using a scintillator and photomultiplier tube and measured as a function of energy (280.0−320.0 eV with a resolution of 0.1 eV) and position (with resolution better than 50 nm). Transmitted X-ray intensity was converted to an X-ray optical density (defined as $OD = \ln(I_0/I)$) by recording the X-ray intensity through a region of the TEM grid with no film. As the intensity of the X-ray beam delivered by the synchrotron varies with energy and time (as the ring current subsides), I_0 was measured as a function of energy for each sample as part of the measurement. In order to provide sufficient data for quantitative analysis, the following protocol was adopted. First the NEXAFS spectra (OD as a function of energy) were recorded for pristine films of PFB and F8BT of known thickness. For each blend film, X-ray images were measured for at least five different X-ray energies, namely 280.0, 284.7, 284.9, 285.1, and 320.0 eV. For each X-ray image acquired, full NEXAFS spectra (typically 259 points between 278 and 320 eV with 0.1 eV resolution between 283 and 298 eV) were also taken at each point along a line section of that image. Care was taken to limit dwell times to avoid potential X-ray damage during scanning. As the aliphatic regions are more susceptible to X-ray damage than the aromatic regions, any significant damage would appear as a poor fit in the 288 eV region of the spectra and as mass loss above 289 eV when fitted/compared to pristine spectra that were taken with a larger spot size to avoid damage. However, we find that our fits still accurately match the blend spectra and that radiation damage does not affect our quantitative analysis.

Quantitative Analysis. Image analysis was assisted by use of the IDL widget aXis2000 (http://unicorn.mcmaster.ca/aXis2000.html). Using the formula $OD(E) = \mu(E)\rho t$ where $\mu(E)$ is the energy-dependent mass absorption coefficient, ρ the film density, and t the film thickness, $\mu(E)$ was calculated for PFB and F8BT from the NEXAFS spectra of the pristine films of known thickness assuming a density of 1 g/cm^3. For calculation of the effective thickness of PFB and F8BT at a given point in a blend film, however, only the product of $\mu(E)$ and ρ needs to be known, which is gained from the pristine NEXAFS spectra with known film thickness. For a blend film, the X-ray optical density measured at a particular point can be considered to be the sum of contributions from PFB and F8BT. Provided the X-ray optical density is known as a function of position for at least two energies, the appropriate simultaneous equations expressing the total X-ray optical density in terms of the sum of contributions from PFB and F8BT can be solved to yield the thickness of the principal components for each point. In this way PFB and F8BT thickness maps were calculated. Assuming equal polymer densities, chemical weight % composition maps were calculated by dividing each thickness image by the total thickness image. As image analysis based on only a few points can introduce unnecessary error, final determination of chemical composition was derived from the NEXAFS spectra line scans. Chemical composition at each point along the line was determined by the least-squares fitting of the blend spectra to a sum of the pristine spectra. For each point the NEXAFS blend spectra were found to be fitted well by a linear combination of the pristine spectra, indicating that there is no ground state intermixing of the π^* orbitals. From these line scans the composition images were rescaled to match the more accurate fit determined from the spectral fits. Further details of the data analysis can be found in our previous communication.[19]

Total Electron Yield (TEY) NEXAFS Measurements. TEY NEXAFS measurements were performed at beamline 10-1 of the Stanford Synchrotron Radiation Laboratory, California. Carbon K-edge NEXAFS spectra were obtained with a spectral resolution of about 50 meV at normal (90°), so-called "magic" (50°), and grazing (20°) angles of X-ray incidence. The spectra were measured in total electron yield (TEY) mode by recording the drain current from the sample; the incident photon flux was simultaneously recorded via the drain current from a gold mesh grid located immediately upstream of the sample chamber. The NEXAFS spectra were normalized as detailed by Watts et al.[22] (A schematic of the geometry of the experimental setup can be found in Figure 2a.)

Device Fabrication and Preparation. Films spin-coated on PEDOT:PSS-coated ITO substrates were completed by the evaporation of ∼80 nm of aluminum at less than 10^{-6} mbar followed by encapsulation in a nitrogen glovebox with less than 1 ppm oxygen. In addition to devices made from blends studied using STXM, different weight ratio chloroform devices were also fabricated. All devices were fabricated with an active layer thickness between 80 and 90 nm. External quantum efficiency (EQE) was measured as a function of wavelength at intensities of ∼1 mW/cm^2, with short-circuit current recorded using a Keithley 237 source measure unit (SMU).

Results and Discussion

NEXAFS Spectra. Figure 1 shows NEXAFS spectra of pristine films of PFB and F8BT. The NEXAFS spectrum of PFB is very similar to TFB[19] but shows a slightly higher π^* peak at 285.1 eV and an enhanced peak at 286.2 eV. PFB has a much higher π^* peak than F8BT, with the latter exhibiting a lower energy shoulder with absorption onset at ∼284 eV. Above 287.0 eV the NEXAFS spectra of PFB and F8BT are nearly identical, with the differences in their NEXAFS spectra between 284 and 287 eV providing the basis for chemical contrast.

The fixed sample geometry relative to the incident synchrotron X-ray beam means that contrast in a STXM image could potentially arise from changes in absolute chemical concentration and/or molecular alignment of the polymer species of interest.[23] In order to assess the potential influence of molecular

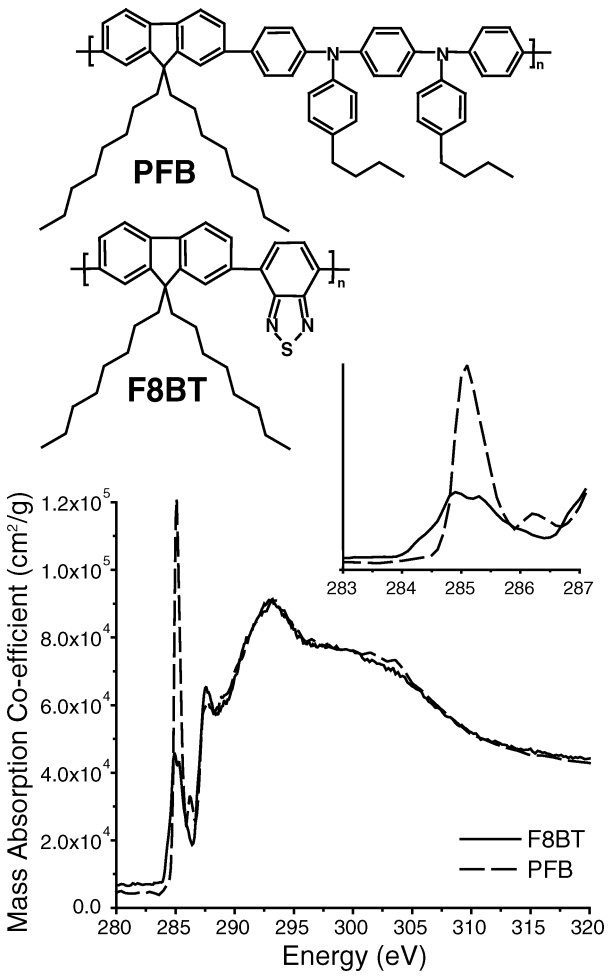

Figure 1. Chemical structures and NEXAFS spectra of pristine films of PFB and F8BT calculated assuming a film density of 1 g/cm^3.

alignment upon our determination of chemical composition, angle-resolved total electron yield (TEY) NEXAFS spectroscopy was performed on pristine PFB, F8BT, and 1:1 xylene blend films (Figure 2). Angle-resolved NEXAFS spectroscopy has previously been applied to probe the molecular alignment of films of the conjugated polymer poly(3-hexylthiophene)[24,25] and is an established method for determining alignment and orientation in such systems. By floating off the blend film from the substrate, both the topside and underside were examined, and since TEY NEXAFS probes only the top 5−10 nm, these measurements also provide information about the chemical composition of the surface layers. The NEXAFS spectra obtained from the pure PFB film showed little variation with angle, indicating that there is a low degree of alignment in pure PFB films, consistent with previous ellipsometric studies.[26] The NEXAFS spectra of pure F8BT films did exhibit a systematic angular dependence, suggesting alignment of the F8BT molecules in the pristine film. The stronger π^* resonance in the 20° F8BT spectrum and stronger F8BT σ^* resonances at normal incidence, shown in Figure 2b, indicate alignment of the F8BT molecules in the pure film such that the ring structures lie within the plane of the film surface (see Figure 2a), in agreement with recent wide-angle X-ray scattering (WAXS) measurements.[27] The NEXAFS spectra of the 1:1 PFB/F8BT films spun from xylene also exhibit a distinct angular dependence, indicating the presence of aligned molecules in these films (Figure 2c). Given that PFB exhibits no alignment effects in the pristine film, it seems reasonable to assume that it does not contribute to the alignment of the blend film. In order to test this

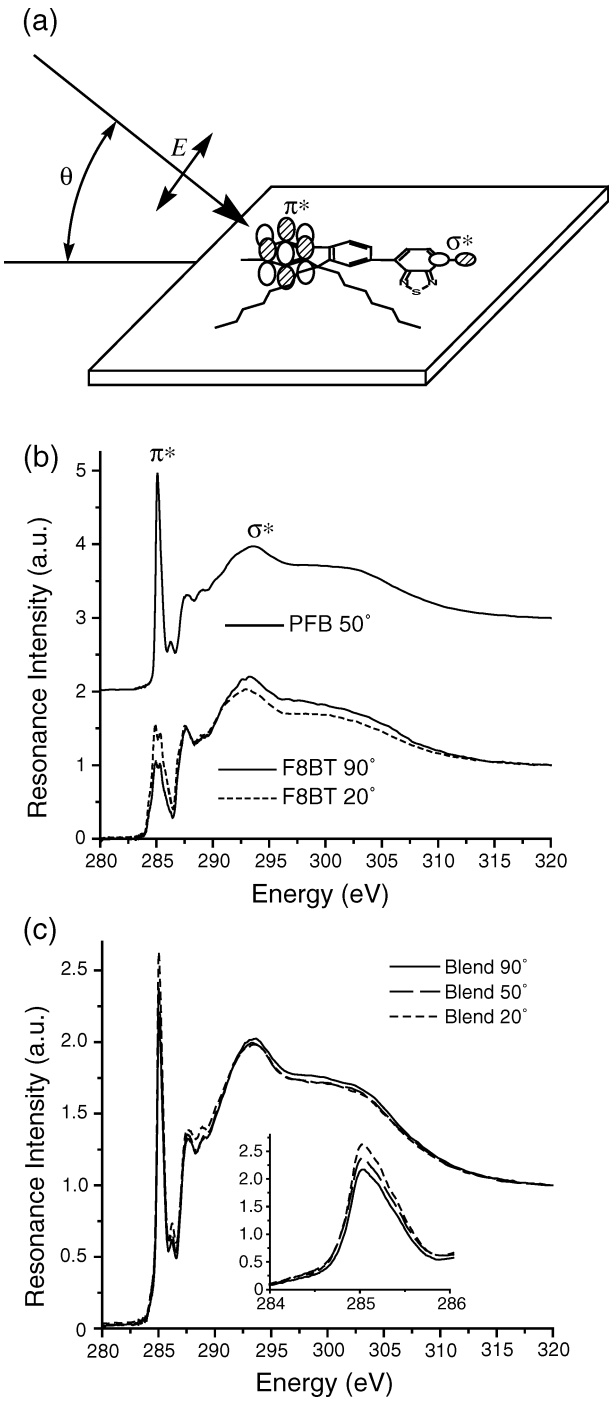

Figure 2. Total electron yield NEXAFS spectra of pristine and blend films of PFB and F8BT as a function of incident X-ray angle. (a) Schematic diagram showing the geometry of the angle-resolved NEXAFS setup, along with the observed preferential orientation of F8BT with schematic π^* and σ^* orbitals. At low angles the electric field vector aligns with the π^* resonance, producing a larger π^* intensity in the NEXAFS spectrum. For normal incidence the electric field vector is orthogonal to the π^* resonance, resulting in a lower π^* NEXAFS signal. The reverse holds for the σ^* orbitals. (b) NEXAFS spectra of pristine PFB and F8BT films. (c) Angle-resolved NEXAFS spectra of a 1:1 xylene blend, with inset showing an enlargement of the π^* region. For all films the X-ray beam was incident upon the topside of the film.

assumption, the pristine PFB spectrum collected at 50° and the F8BT spectra collected at 20° and 90° were least-squares fitted to the NEXAFS blend spectra. The results of this fitting for each angular set of spectra collected for the topside and underside of the blend film are shown in Table 1, and we find that the blend NEXAFS spectra are well-fitted using this

Table 1. Summary of the Fitting Parameters Used To Fit Angle-Resolved Pristine Spectra (PFB-50°, F8BT-90°, and F8BT-20°) to the Angle-Resolved Blend Spectra of the Topside and Underside of a 1:1 Xylene Blend Film

	topside			underside		
component	90°	50°	20°	90°	50°	20°
PFB	0.56	0.58	0.67	0.73	0.76	0.74
F8BT-90°	0.36	0.04	0	0.23	0.11	0
F8BT-20°	0.07	0.38	0.33	0.04	0.13	0.26

approach. In particular, we find that the relative concentration of PFB is enhanced for the underside blend spectra, in good agreement with previous studies that indicated the presence of a PFB wetting layer at the film−substrate interface.[28] More importantly, however, when the blend film is at the extreme angles of 20° and 90°, the corresponding F8BT angular component dominates the overall F8BT contribution to the fit. Therefore, we conclude that the molecular alignment observed in the 1:1 blend film can be entirely attributed to the alignment of the F8BT component and is of a comparable magnitude and the same orientation to that measured in the pristine F8BT film. As such, any contrast observed in the STXM maps can be entirely attributed to changes in the chemical composition of the blend films rather than to relative changes in alignment of the individual components.

X-ray Images and Film Structure. Figure 3 shows PFB and F8BT chemical composition images compared to AFM images of 1:1, 5:1, and 1:5 blend films spin-coated from xylene. The domain sizes observed by AFM match those seen by STXM confirming that they are columnar in nature.[15] Examining the STXM images of the 1:1 PFB:F8BT blend film (Figure 3a,b) and the associated cross-sectional traces (Figure 4) reveals that the 1:1 blend shows similar features to 1:1 poly(9,9′-dioctylfluorene-*co*-*N*-(4-butylphenyl)diphenylamine) (TFB)/F8BT blends utilized in polymer LEDs reported previously.[19] In particular, (i) the PFB-rich domain is uniformly mixed (discounting the small F8BT-rich droplets less than 500 nm wide) with a composition of 70 ± 3 wt % PFB; (ii) the F8BT domain is much purer than the PFB domain, with a composition of up to 95 wt % F8BT; (iii) the composition of the F8BT-rich domain is not uniform, with the F8BT concentration decreasing slightly with increasing distance from the interface; (iv) subsurface PFB-rich droplets are observed in the F8BT-rich domain for thicker films (not shown); and (v) the width of the domain interface as measured from the line scans (Figure 4) is 200 nm.

Turning now to the 1:5 and 5:1 blends, a general feature of both blends is that the enclosed minority phases are not pure (Figure 3d,h). Examining the cross-sectional traces displayed in Figure 5 reveals that for both blends the composition of the minor phase approaches a 1:1 composition.[29] A subtle difference between these two blends, however, is the degree of purity of the surrounding majority phases. While the PFB-rich phase in the 5:1 blend contains roughly 10 wt % F8BT, the proportion of PFB in the F8BT-rich phase of the 1:5 blend drops virtually

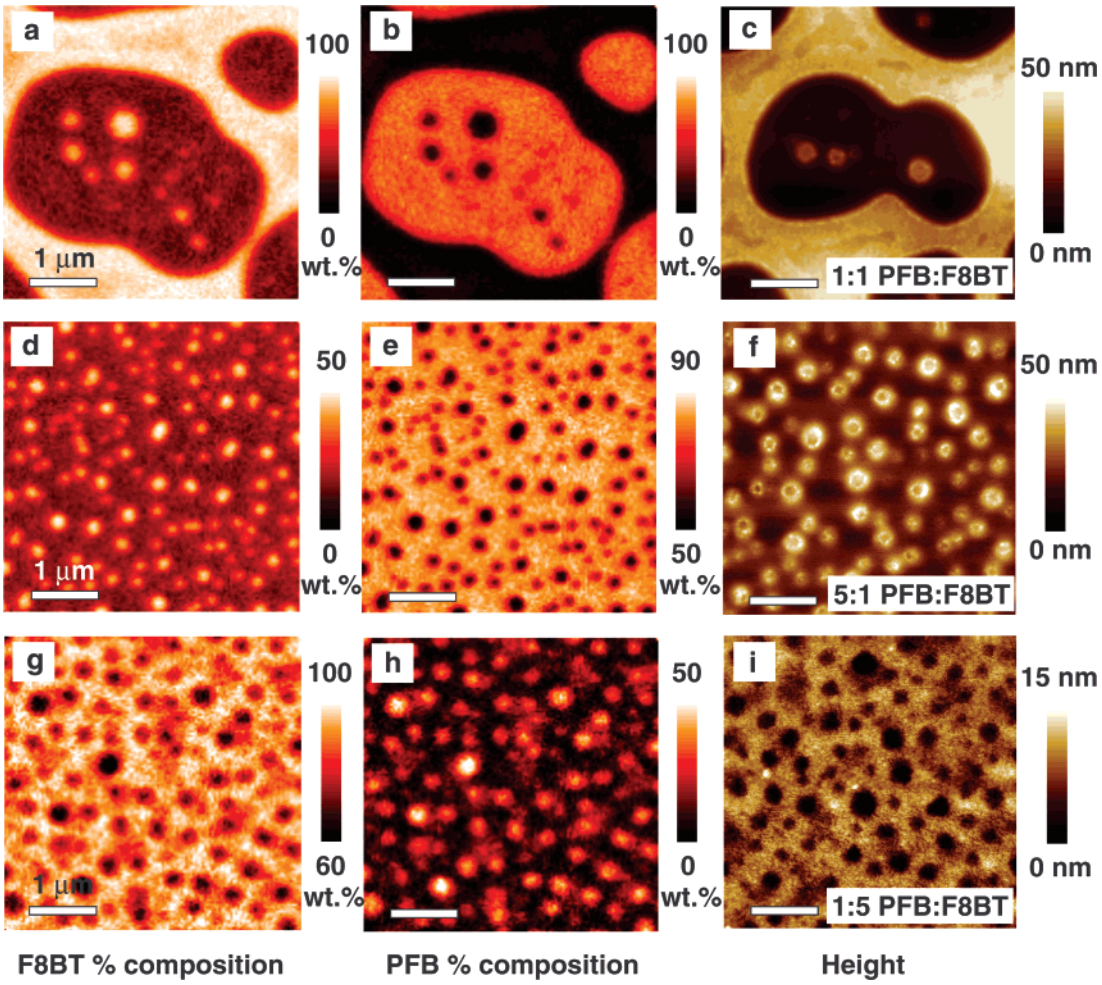

Figure 3. 5 μm by 5 μm STXM composition maps (left and center columns) and AFM images (right column) of PFB/F8BT blend films. The left column shows F8BT wt % composition maps while the center column shows PFB wt % composition maps. (a), (b), and (c) are of a 1:1 PFB:F8BT blend film; (d), (e), and (f) are of a 5:1 PFB:F8BT blend film; (g), (h), and (i) are of a 1:5 PFB:F8BT blend film.

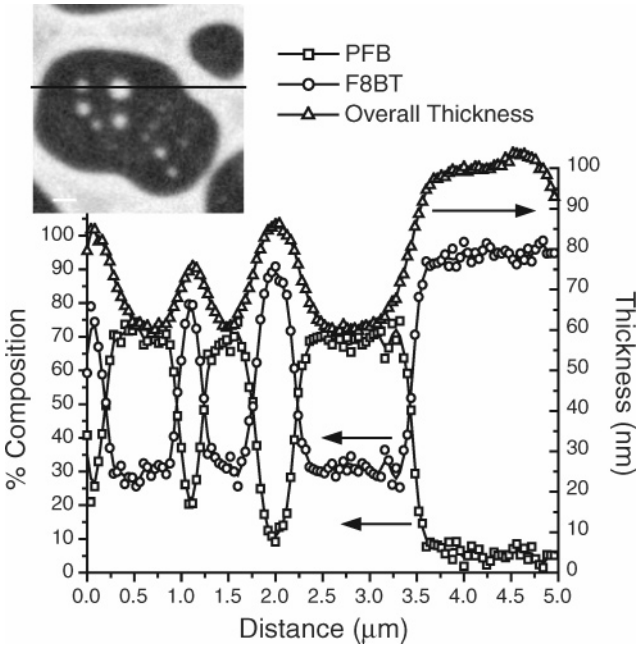

Figure 4. Cross-sectional wt % composition and thickness traces of the 1:1 blend. Each data point represents the result of the least-squares fit of pristine spectrum to a full NEXAFS spectrum acquired at that point. Film thickness was determined from the X-ray absorption at the chemically insensitive energy of 320 eV.

to zero between PFB-rich domains. This difference in majority phase purity is consistent with the STXM results for the 1:1 blend where the PFB-rich domain is observed to be more intermixed than the F8BT domain. The observed differences in purity may be related to the different solubilities of PFB and F8BT[28] or to differences in molecular packing of the F8BT and PFB monomers that may produce different entropies of mixing for F8BT-rich and PFB-rich domains.[30] The data also show that the 1:5 blend does not possess an extensive PFB-rich wetting layer consistent with the observation by Higgins et al. that no poly(9,9′-dioctylfluorene) (F8) wetting layer is detected by NRA in similar weight ratio blends of F8 with F8BT (92 wt % F8BT).

Figure 6 shows a STXM image recorded at 285.1 eV of a 1:1 blend film prepared from chloroform and reveals that no features can be seen on a length scale greater than 50 nm, confirming that the blend is well mixed. (Note that the graininess of the image is due to noise that exhibits a Gaussian distribution. Many other images of this blend were taken at different energies with no correlation between image features in the different scans.) These results demonstrate that there is no additional lateral subsurface structure on a length scale of 50 nm or more and agree with previous AFM and NRA observations indicating a featureless surface morphology[6] and a uniform composition normal to the substrate,[31] respectively. Figure 6 also shows the NEXAFS spectra of the blend and least-squares fit to the pristine spectra indicating a composition of 47 ± 3 wt % PFB, in agreement with the solution blend ratio. This agreement provides an independent confirmation that our NEXAFS measurements are indeed accurately measuring chemical composition in blend films and are not skewed by changes in molecular alignment.

Correlating Device Performance with Film Composition. In order to probe the relationships between morphology and device performance, devices have been fabricated from films prepared under identical conditions to those prepared for STXM analysis. Figure 7 shows the measured external quantum efficiency for organic photovoltaic devices based on 1:1 xylene, 5:1 xylene, 1:5 xylene, and 1:1 chloroform PFB/F8BT films.

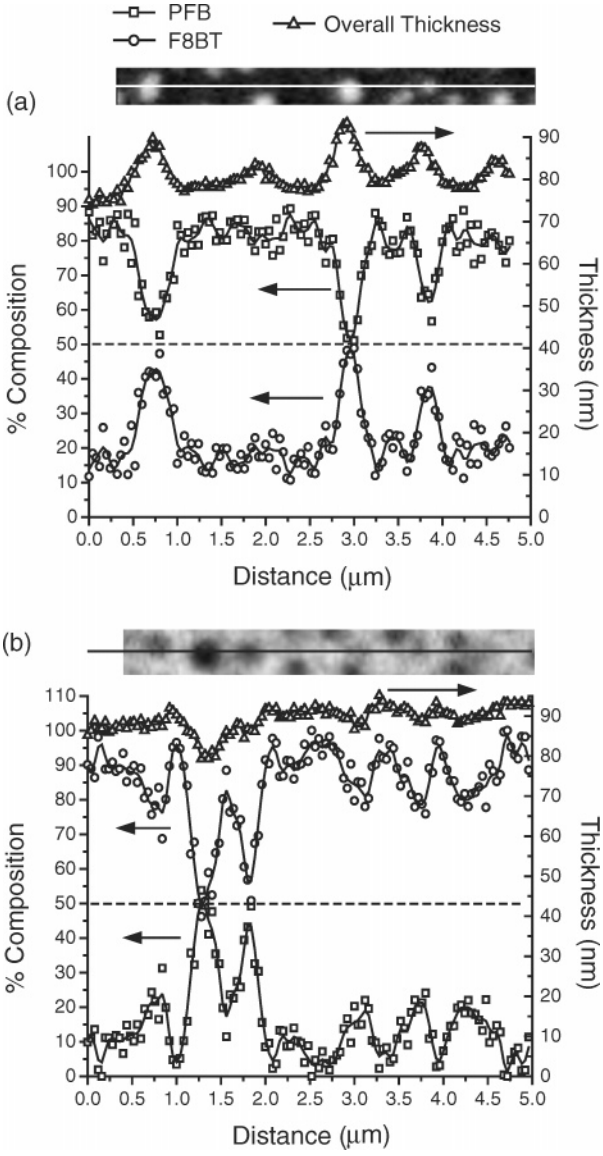

Figure 5. Cross-sectional wt % composition and thickness traces of (a) 5:1 and (b) 1:5 blend xylene processes PFB:F8BT blends. The composition of the minority phases in (a) and (b) approaches a 1:1 composition as indicated by the dashed lines.

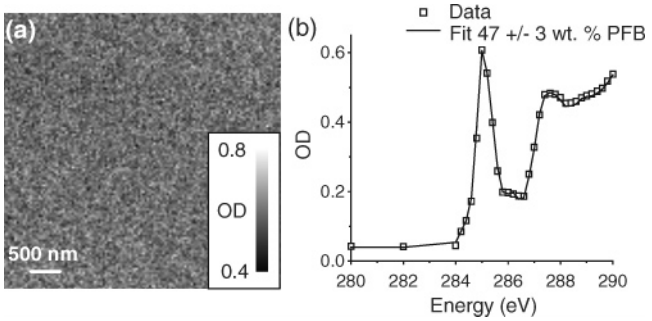

Figure 6. (a) STXM image of a 1:1 chloroform blend image acquired at 285.1 eV. (b) NEXAFS spectra of the chloroform blend film (squares) with the least-squares fit to the sum of pristine spectra.

As expected, the chloroform device is the most efficient, followed by the 1:5 xylene blend, the 5:1 xylene blend, and finally the 1:1 xylene blend, with the trend in xylene-processed devices agreeing with previous measurements.[7]

As a model system for understanding the influence of local variations in composition on overall device performance,

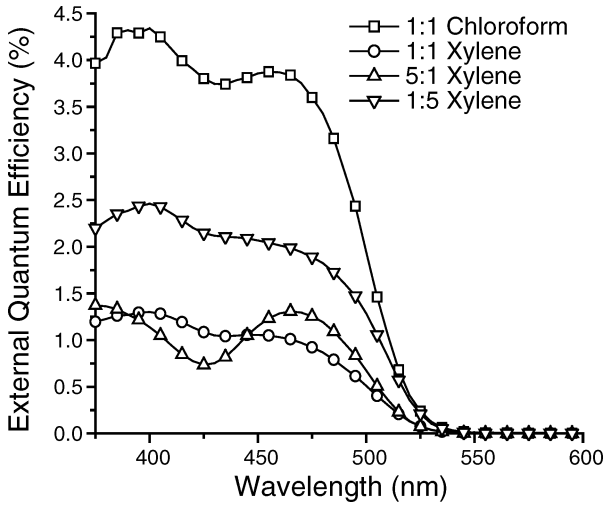

Figure 7. Spectral response of the external quantum efficiency of PFB/F8BT blend devices.

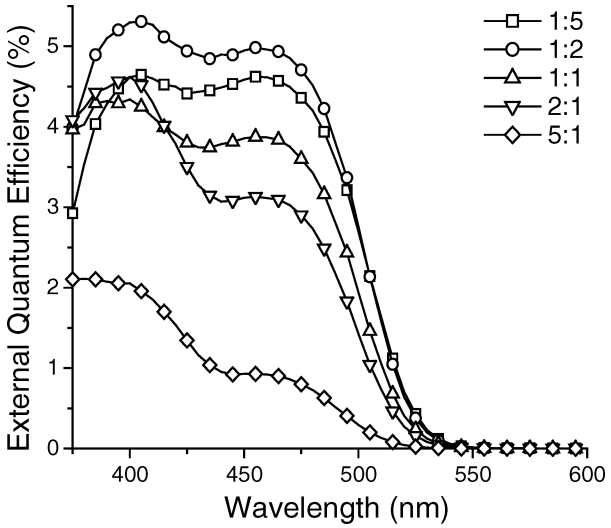

Figure 8. Comparison of chloroform-processed devices with different PFB:F8BT weight ratios.

chloroform-processed devices that possess a uniform morphology throughout the entire active layer have been fabricated with various weight ratios. Figure 8, which plots EQE as a function of composition for these devices, reveals that blends with a moderate excess of F8BT produce more efficient devices. This improvement in efficiency with increased F8BT content can be understood in terms of a gradient of photoexcitations within the device due to illumination through the ITO electrode. Thus, once a photoexcitation is separated, electron transport through F8BT networks to the cathode is more critical to device performance than hole transport through PFB networks to the anode. With knowledge of how device function varies with composition, as measured for these chloroform-processed devices, it is possible to calculate the expected macroscopic efficiencies of the xylene-processed devices based on the locally measured composition distributions of each xylene blend. Figure 9a shows histograms of the number of pixels (i.e., relative area) vs % F8BT composition from each of the % F8BT images in Figure 3. These composition distributions were then multiplied by a fitted curve expressing external quantum efficiency at the F8BT absorption peak (465 nm) as a function of F8BT content based on the data of Figure 8 and integrated to produce the expected macroscopic efficiency of each xylene blend.

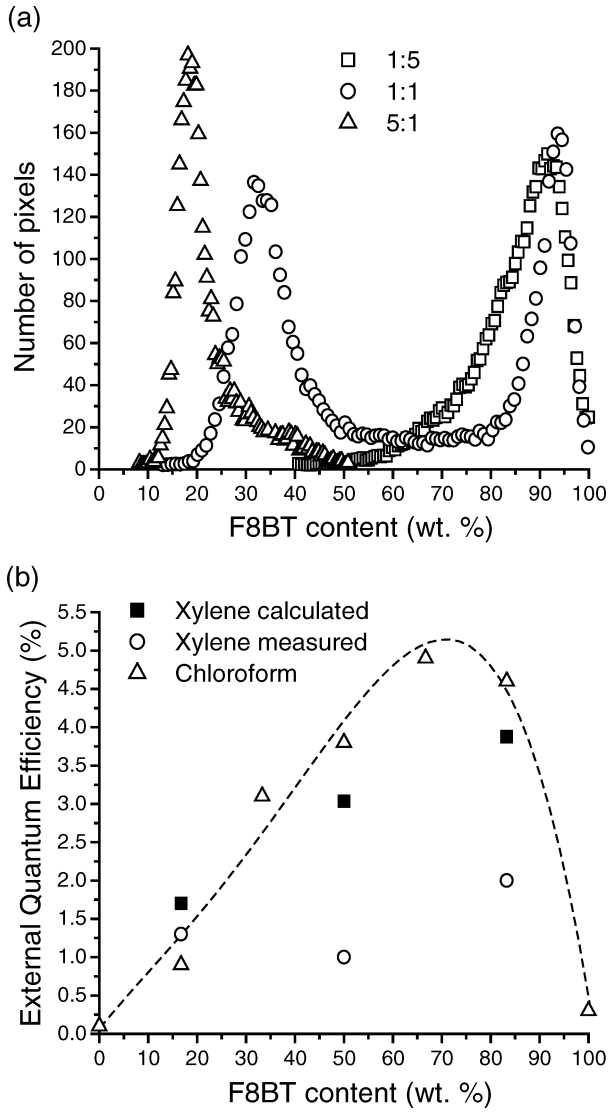

Figure 9. (a) Distribution of local blend composition of 1:5 (squares), 1:1 (circles), and 5:1 (triangles) xylene-processed blend films determined from Figure 3. (b) Calculated efficiencies of xylene-processed blends (squares) based on the distribution of local blend composition compared to the measured efficiencies of xylene-processed devices (circles) and chloroform devices (triangles; data points for pure PFB and F8BT devices taken from Arias[33] and Snaith et al.[7]), all at a wavelength of 465 nm. The dashed line shows the fit to the chloroform data used to calculate the xylene efficiencies.

Figure 9b presents the calculated macroscopic efficiencies of the xylene blends together with the measured efficiencies of the xylene and chloroform blends with 465 nm incident light. Here, we can clearly see that in general the performance of the xylene-processed devices is much less than expected when considering local blend composition alone. However, the model does explain why the 1:5 blend outperforms the 5:1 blend as the former has a higher proportion of device area with composition lying in the optimum 60−80% F8BT range (see Figure 9a). The model also explains why the 5:1 xylene blend outperforms the 5:1 chloroform blend, since the xylene blend has regions with higher F8BT content with improved efficiency. While the model predicts the relative efficiencies of the 1:5 and 5:1 xylene blends, the performance of the 1:1 xylene blend is counter to the trend predicted by the model. The lower than expected measured performance of the 1:1 blend, however, can be explained by the existence of vertical film structure not probed by STXM and hence unaccounted for by the model.

Chiesa et al. have demonstrated, using scanning Kelvin probe microscopy, that a PFB-rich capping layer exists on top of the F8BT-rich domain in 1:1 blends processed from xylene and that the presence of this capping layer reduces device efficiency by blocking the transport of photogenerated electrons to the surface.[32] Thus, the limited efficiency of the F8BT-rich domains in 1:1 blends processed from xylene will further reduce the macroscopic efficiency of 1:1 xylene blend devices in a way unaccounted for by the model presented in Figure 9.

The overall discrepancy between predicted and measured efficiencies when considering local blend composition alone indicates that ultimately there is another factor that determines the poor performance of xylene blends compared to chloroform blends. The large difference in the boiling points of xylene and chloroform means that these blends will differ not only in the degree of micron-scale phase separation but also in the degree of nanoscale phase separation. As xylene-processed films experience an extended drying time relative to chloroform-processed films, both nanoscale and micron-scale phase separation of xylene-processed films will be more evolved than that of chloroform-processed films. This difference in the degree of nanoscale morphology is reflected by the differences in absolute photoluminescence efficiencies of xylene-processed blends (10−20%[7]) compared to that of chloroform-processed blends (2−4%[33]). As the absolute photoluminescence efficiencies of pure films of PFB and F8BT are around 30−50%, a significant proportion of excitons are not dissociated in xylene-processed blend films. In contrast, chloroform blends exhibit 5 times more efficient photoluminescence quenching than xylene blends. Thus, the more evolved phase-separation in xylene blends results in a significantly lower exciton dissociation efficiency and accounts for the lower overall efficiency of xylene-processed blends compared to chloroform-processed blends.

Having explained the relative performance of xylene-processed devices by considering the local blend composition distributions of Figure 9a, it is worth now relating the measured composition images of Figure 3 to local photocurrent generation efficiency. Since areas with high F8BT concentration are expected to produce more photocurrent, the major phase in the 1:5 blend is expected to be more efficient than the enclosed minor phase. Similarly, the minor phase in the 5:1 blend is expected to be more efficient than the surrounding major phase. This assignment is consistent with the electrostatic force microscopy (EFM) measurements by Coffey and Ginger[17] that found higher charging rates for the F8BT-rich domains. For the 1:1 blend, the situation is complicated by the presence of the PFB-rich capping layer that limits the efficiency of the F8BT-rich phase. Nonetheless, efficient operation may be expected from the areas of the F8BT-rich domain closest to the domain interface lacking a PFB capping layer.[32] However, this region has higher than optimum F8BT content (>90%) and may have efficiency comparable to that of the 30% F8BT PFB-rich domain, especially when differences in domain thickness are accounted for. While near-field scanning photocurrent studies found that the PFB-rich domain is more efficient,[16] EFM studies found similar intradomain efficiencies for the two domains.[17] The difference between these measurements may be related to the different direction of illumination for the two techniques[16] or indeed due to differences in polymer batches. Differences in the molecular weights of the polymers used in this study (>100 000 g/mol) compared to those used in the EFM study (<40 000 g/mol) would also have a strong influence on the resulting morphologies, explaining the different macroscale morphologies observed for higher F8BT content films.

Conclusions

We have quantitatively mapped the blend composition of PFB:F8BT blends using scanning transmission X-ray microscopy. We find that for xylene-processed films the micron-scale domains in general still contain significant proportions of both polymers. In particular, for 1:5 and 5:1 xylene blend films the minority phase is not pure but can contain up to 50% of each polymer. By studying the distribution of local blend composition in xylene-processed films, we explain the superior performance of 1:5 blends compared to 5:1 blends by the higher proportion of the 1:5 film that have the optimum 60−80 wt % F8BT blend composition. The distribution of local blend composition in 1:1 xylene-processed films, however, was unable to explain the lower performance of the 1:1 blend, which is ultimately attributed to additional vertical structure. Overall, the lower performance of xylene-processed films relative to chloroform-processed films cannot be accounted for by local blend composition alone but must be explained by differences in the degree of finer nanoscale phase separation.

Acknowledgment. The authors thank the ALS for beamtime, David Kilcoyne and Tohru Araki for technical assistance, and Adam Hitchcock and for fruitful discussions. This work was supported by the Engineering and Physical Sciences Research Council, U.K. (SUPERGEN IV), and by the Australian Research Council's Discovery funding scheme (DP0559417). We acknowledge financial support from the Commonwealth of Australia through the Access to Major Research Facilities Program. The ALS is supported by the Director, Office of Science, Office of Basic Energy Sciences, of the U.S. Department of Energy under Contract DE-AC02-05CH11231. Portions of this research were carried out at the Stanford Synchrotron Radiation Laboratory, a national user facility operated by Stanford University on behalf of the U.S. Department of Energy, Office of Basic Energy Sciences. The authors also thank Cambridge Display Technology Ltd. for the supply of conjugated polymers used in this study.

References and Notes

(1) Halls, J. J. M.; Walsh, C. A.; Greenham, N. C.; Marseglia, E. A.; Friend, R. H.; Moratti, S. C.; Holmes, A. B. *Nature (London)* **1995**, *376*, 498−500.
(2) Yu, G.; Heeger, A. J. *J. Appl. Phys.* **1995**, *78*, 4510.
(3) Hoppe, H.; Sariciftci, N. S. *J. Mater. Chem.* **2006**, *16*, 45−61.
(4) Halls, J. J. M.; Pichler, K.; Friend, R. H.; Moratti, S. C.; Holmes, A. B. *Appl. Phys. Lett.* **1996**, *68*, 3120.
(5) Coakley, K. M.; McGehee, M. D. *Chem. Mater.* **2004**, *16*, 4533−4542.
(6) Arias, A. C.; MacKenzie, J. D.; Stevenson, R.; Halls, J. J. M.; Inbasekaran, M.; Woo, E. P.; Richards, D.; Friend, R. H. *Macromolecules* **2001**, *34*, 6005−6013.
(7) Snaith, H. J.; Arias, A. C.; Morteani, A. C.; Silva, C.; Friend, R. H. *Nano Lett.* **2002**, *2*, 1353−1357.
(8) Halls, J. J. M.; Arias, A. C.; MacKenzie, J. D.; Wu, W.; Inbasekaran, M.; Woo, E. P.; Friend, R. H. *Adv. Mater.* **2000**, *12*, 498−502.
(9) Watkins, P. K.; Walker, A. B.; Verschoor, G. L. B. *Nano Lett.* **2005**, *5*, 1814−1818.
(10) Snaith, H. J.; Friend, R. H. *Thin Solid Films* **2004**, *451*−*452*, 567−571.
(11) Snaith, H. J.; Greenham, N. C.; Friend, R. H. *Adv. Mater.* **2004**, *16*, 1640−1645.
(12) Morteani, A. C.; Dhoot, A. S.; Kim, J. S.; Silva, C.; Greenham, N. C.; Murphy, C.; Moons, E.; Ciná, S.; Burroughes, J. H.; Friend, R. H. *Adv. Mater.* **2003**, *15*, 1708−1712.
(13) Morteani, A. C.; Sreearunothai, P.; Herz, L. M.; Friend, R. H.; Silva, C. *Phys. Rev. Lett.* **2004**, *92*, 7402.
(14) Pacios, R.; Bradley, D. D. C. *Synth. Met.* **2002**, *127*, 261−265.
(15) Ramsdale, C. M.; Bache, I. C.; MacKenzie, J. D.; Thomas, D. S.; Arias, A. C.; Donald, A. M.; Friend, R. H.; Greenham, N. C. *Physica E* **2002**, *14*, 268−271.

(16) McNeill, C. R.; Frohne, H.; Holdsworth, J. L.; Dastoor, P. C. *Nano Lett.* **2004**, *4*, 2503−2507.
(17) Coffey, D. C.; Ginger, D. S. *Nat. Mater.* **2006**, *5*, 735−740.
(18) Moons, E. *J. Phys.: Condens. Matter* **2002**, *14*, 12235−12260.
(19) McNeill, C. R.; Watts, B.; Thomsen, L.; Belcher, W. J.; Greenham, N. C.; Dastoor, P. C. *Nano Lett.* **2006**, *6*, 1202−1206.
(20) Heriot, S. Y.; Jones, R. A. L. *Nat. Mater.* **2005**, *4*, 782−786.
(21) Kilcoyne, A. L. D.; Tyliszczak, T.; Steele, W. F.; Fakra, S.; Hitchcock, P.; Franck, K.; Anderson, E. H.; Harteneck, B. D.; Rightor, E. G.; Mitchell, G. E.; Hitchcock, A. P.; Yang, L.; Warwick, T.; Ade, H. *J. Synchrotron Rad.* **2003**, *10*, 125−136.
(22) Watts, B.; Thomsen, L.; Dastoor, P. C. *J. Electron Spectrosc. Relat. Phenom.* **2006**, *151*, 105−120.
(23) Stöhr, J. *NEXAFS Spectroscopy*; Springer: Berlin, 1992.
(24) DeLongchamp, D. M.; Sambasivan, S.; Fischer, D. A.; Lin, E. K.; Chang, P.; Murphy, A. R.; Fréchet, J. M. J.; Subramanian, V. *Adv. Mater.* **2005**, *17*, 2340−2344.
(25) DeLongchamp, D. M.; Vogel, B. M.; Jung, Y.; Gurau, M. C.; Richter, C. A.; Kirillov, O. A.; Obrzut, J.; Fischer, D. A.; Sambasivan, S.; Richter, L. J.; Lin, E. K. *Chem. Mater.* **2005**, *17*, 5610−5612.
(26) Ramsdale, C.; Greenham, N. C. *J. Phys. D: Appl. Phys.* **2003**, *36*, L29−L34.
(27) Donley, C. L.; Zaumseil, J.; Andreasen, J. W.; Nielsen, M. M.; Sirringhaus, H.; Friend, R. H.; Kim, J. S. *J. Am. Chem. Soc.* **2005**, *127*, 12890−12899.
(28) Kim, J. S.; Ho, P. K. H.; Murphy, C. E.; Friend, R. H. *Macromolecules* **2004**, *37*, 2861−2871.
(29) We have considered the potential effect of the finite spot size of the STXM beam on the observed intermixing of the submicron domains but find that our observations are not substantially influenced.
(30) Jones, R. A. L.; Richards, R. W. *Polymers at Surfaces and Interfaces*; Cambridge University Press: Cambridge, 1999.
(31) Higgins, A. M.; Martin, S. J.; Thompson, R. L.; Chappell, J.; Voigt, M.; Lidzey, D. G.; Jones, R. A. L.; Geoghegan, M. *J. Phys.: Condens. Matter* **2005**, *17*, 1319−1328.
(32) Chiesa, M.; Burgi, L.; Kim, J. S.; Shikler, R.; Friend, R. H.; Sirringhaus, H. *Nano Lett.* **2005**, *5*, 559−563.
(33) Arias, A. C. Ph.D. Thesis, University of Cambridge, 2001.

MA070132D